

# BUSTING UP BINARIES: ENCOUNTERS BETWEEN COMPACT BINARIES AND A SUPERMASSIVE BLACK HOLE

ERIC ADDISON

Department of Physics, Utah State University, Logan, UT 84322, USA.

PABLO LAGUNA

Center for Relativistic Astrophysics and School of Physics,  
School of Physics, Georgia Institute of Technology, Atlanta, GA 30332, USA.

SHANE L. LARSON

Center for Interdisciplinary Exploration and Research in Astrophysics,  
Northwestern University, Evanston, IL 60208, USA  
and Department of Astronomy, Adler Planetarium, Chicago, IL 60605 USA.

*Draft version August 6, 2018*

## ABSTRACT

Given the stellar density near the galactic center, close encounters between compact object binaries and the supermassive black hole are a plausible occurrence. We present results from a numerical study of close to 13 million such encounters. Consistent with previous studies, we corroborate that, for binary systems tidally disrupted by the black hole, the component of the binary remaining bound to the hole has eccentricity  $\sim 0.97$  and circularizes dramatically by the time it enters the classical LISA band. Our results also show that the population of surviving binaries merits attention. These binary systems experience perturbations to their internal orbital parameters with potentially interesting observational consequences. We investigated the regions of parameter space for survival and estimated the distribution of orbital parameters post-encounter. We found that surviving binaries harden and their eccentricity increases, thus accelerating their merger due gravitational radiation emission and increasing the predicted merger rates by up to 1%.

## 1. INTRODUCTION

Observations of gravitational waves (GWs) will allow us to probe dynamical astrophysical systems in regimes where strong gravity plays a key role. In galactic nuclei, GWs from stellar mass interactions with a supermassive black hole (SMBH) will be excellent probes of the properties of the SMBH and the stellar population itself. It is thus important to investigate the types of encounters that should be expected as well as the strength and frequency of GWs emitted by these events.

In the present work, we will focus on encounters between stellar mass binaries and a galactic SMBH. Previous studies have focused on the hyper-velocity star (HVS) produced by the disruption of the binary and stellar collisions (Hills 1988; Gualandris et al. 2005; Antonini et al. 2010). Miller et al. (2005) investigated the eccentricity of the bound component created by the binary disruption, namely the extreme mass-ratio inspiral (EMRI) left behind. More recently, binary interactions with SMBH have been explored in the context of the GW emissions in the LIGO band from binaries driven to merger by Kozai resonance (Antonini & Perets 2012; Antonini et al. 2014).

The strongest GW sources will involve compact, degenerate stellar remnants that can survive close encounters with the central black hole, namely neutron stars and stellar mass black hole (BH)s. The fraction of field stars in binaries varies by stellar type, but for O- and B-type stars, which are the stellar types massive enough to form neutron stars or BHs, it is estimated that more

than 75% of O-type and 70% of B-type stars have some number of companions (Raghavan et al. 2010). Near the galactic center, the density of stars grows very large compared to field conditions, with density estimates up to  $10^8 M_{\odot} \text{pc}^{-3}$  within the inner 0.1pc, (Alexander 2005). Given this information, it is reasonable to expect the existence of compact object (CO) binaries in the galactic center, and in fact it has been observed by way of X-ray transients that CO binaries exist near the GC, and are more abundant within the inner 1 pc (Muno et al. 2005). It has been estimated that as many as  $\sim 20,000$  stellar mass BH binaries have segregated within the inner  $\approx 1$  pc of the Milky Way galactic center (O’Leary et al. 2009).

With the existence of CO binaries near the galactic center, it is reasonable to expect that some number of them may interact directly with the SMBH. Many known main sequence stars exist in bound orbits around the SMBH (Ghez et al. 2005, 2008, 2009), suggesting that the same could be true for COs and CO binaries. Such interactions have implications for GW campaigns of observations, for example ground based observatories (e.g. LIGO) searching for compact binary coalescences (CBCs). Proposed space based interferometers (e.g. LISA) will be sensitive to EMRIs which can be created by the tidal disruption of CO binaries near the SMBH.

In the present study, we corroborate and extend the results of Miller et al. (2005) for the formation of EMRIs by tidal disruption to arbitrary binary orientations. In

addition, we focus our attention on those binary systems that survive the encounter with the SMBH. In particular, we investigate whether those binaries are able to survive and face subsequent encounters before merging from GW emission or merge faster than those not experiencing encounters with SMBH, and discuss the implication of the encounters on predicted CBC rates. We concentrate on initially circular, equal mass ( $m_1 = m_2 \equiv m$ ), CO binaries approaching the SMBH in a parabolic orbit. We vary the orientation of the orbital angular momentum of the CO binary relative to the angular momentum of the CO binary orbiting the SMBH. We also vary the pericenter distance  $r_p$  between the CO binary and the SMBH. Our study explores a greater volume of the parameter space; Antonini & Perets (2012) focused on binaries bound to the SMBH at a fixed orientation, and Miller et al. (2005) explored hyperbolic encounters with coplanar binaries. Considering a larger region of parameter space comes at the expense of integration sophistication, though the time and distance scales involved in our simulation suggest that relativistic effects will not play a significant role for the majority of the parameter range, and Newtonian gravitational forces should suffice.

The paper is organized as follows: Section 2 outlines the outcomes of the three body encounters based on energy arguments. In Section 3, we describe the setup of the encounters. Parameter probability distributions and an estimate of the tidal radius are given in section 4. The analysis of the disrupted binaries is found in Section 5. In Section 6, we discuss the results of those binaries that survived the encounter with the SMBH. Section 7 includes a discussion of the changes in the lifetime of the CO binary due to GW emission as a result of the encounter with the hole as well as consequences to GW detection rates for CO binaries. The paper ends with conclusions in Section 8.

## 2. ENERGETICS AT A GLANCE

The total energy for a three-body system can be written as

$$E = \frac{1}{2} \sum_{i=1}^3 m_i v_i^2 - \sum_{i=1}^2 \sum_{j=i+1}^3 \frac{G m_i m_j}{|\mathbf{r}_i - \mathbf{r}_j|} \quad (1)$$

In the barycentric frame, with  $M_b = m_1 + m_2$  the mass of the binary and  $M_\bullet = m_3$  the mass of the SMBH, the total energy reads

$$E = \frac{1}{2} \frac{M_b M_\bullet}{M_b + M_\bullet} \mathbf{V}^2 - \sum_{i=1}^2 \frac{G m_i M_\bullet}{|\mathbf{r}_i - \mathbf{r}_3|} + E_b. \quad (2)$$

Above,

$$E_b = \frac{1}{2} \mu v^2 - \frac{G \mu M_b}{r} \quad (3)$$

is the internal energy of the binary with  $\mathbf{r} = \mathbf{r}_1 - \mathbf{r}_2$ ,  $\mathbf{v} = \mathbf{v}_1 - \mathbf{v}_2$  and  $\mu = m_1 m_2 / M_b$ . Furthermore,

$$\mathbf{V} = \mathbf{v}_3 - \frac{1}{M_b} \sum_{i=1}^2 m_i \mathbf{v}_i \quad (4)$$

is the relative velocity between the binary and the SMBH. Since  $M_\bullet \gg M_b$ , we can set  $\mathbf{r}_3 = 0$  and ap-

proximate  $\mathbf{v}_3 \approx 0$ . The total energy thus become

$$E = \frac{1}{2} M_b V_b^2 - \sum_{i=1}^2 \frac{G m_i M_\bullet}{r_i} + E_b. \quad (5)$$

where  $V_b$  is the velocity of the center-of-mass of the binary relative to the SMBH. Since for the incoming binary  $R \gg r$ , with  $R$  denoting the distance of the center-of-mass of the binary to the SMBH, we can rewrite the total energy as

$$E \approx \frac{1}{2} M_b V_b^2 - \frac{G M_b M_\bullet}{R} + E_b = E_{cm} + E_b. \quad (6)$$

As mentioned before, we inject the binaries in parabolic orbits; therefore, the initial center of mass energy of the binary with the black hole is  $E_{cm,0} = 0$ . Therefore, the total energy is given by the initial internal binding energy of the binary,  $E = E_{b,0} < 0$ .

The effect of the encounter is to re-distribute the energy available, i.e.  $E_{b,0}$ , among the three bodies. If the binary survives,  $E_b < 0$ . Given that

$$E = E_{cm} + E_b = E_{b,0} < 0, \quad (7)$$

the CO binary after the encounter could be bound ( $E_{cm} < 0$ ) or unbound ( $E_{cm} > 0$ ) to the SMBH.

On the other hand, if the CO binary does not survive ( $E_b > 0$ ), the separation  $r$  of its components will grow; thus, one can neglect in Eq. (1)

$$\frac{G m_1 m_2}{|\mathbf{r}_2 - \mathbf{r}_1|} \approx 0, \quad (8)$$

and rewrite the total energy as

$$E = \sum_{i=1}^2 \left( \frac{1}{2} m_i v_i^2 - \frac{G m_i M_\bullet}{r_i} \right) = \sum_{i=1}^2 E_i, \quad (9)$$

where we have used again that  $\mathbf{r}_3 = 0$  and  $\mathbf{v}_3 \approx 0$ . Therefore, for CO binaries that are disrupted

$$E = E_1 + E_2 = E_{b,0} < 0. \quad (10)$$

The possible outcomes in this situation are both COs bound to the SMBH ( $E_1, E_2 < 0$ ), or one bound and the other unbound ( $E_i < 0 < E_j$ ). Clearly, the case in which bound components are unbound ( $0 < E_1, E_2$ ) is not possible.

We will refer to a CO binary in a bound orbit around a SMBH as a binary extreme mass-ratio inspiral (BEMRI), and will classify the aftermath of the binary from the encounter with the SMBH into one of the following four classes:

- DB: Disrupted binary.
- Long BEMRI: Survived binary bound to SMBH with  $\tau_{\text{gw}} > P_\bullet$ .
- Short BEMRI: Survived binary bound to SMBH with  $\tau_{\text{gw}} < P_\bullet$ .
- SU: Survived binary unbound to the hole.

In this classification,  $\tau_{\text{gw}}$  refers to the binary merger lifetime from GW emission, the so-called Peters lifetime (Peters 1964), and  $P_\bullet$  is the period of the bound binary around the SMBH. One of the main motivations of our study is to investigate how the probability of a binary

falling into one of these categories could alter the predicted CBC.

The fate of a CO binary encountering a SMBH depends on its *penetration factor*  $\beta$ . The penetration factor is defined as the ratio  $\beta \equiv r_t/r_p$ , where  $r_t$  is the *tidal radius* and  $r_p$  the distance of closest approach to the SMBH. In analogy with the common definition of tidal radius for the stellar disruption of stars by massive BHs, we define the tidal radius  $r_t$  as

$$r_t \equiv \left(\frac{M_\bullet}{M_b}\right)^{1/3} a_0, \quad (11)$$

where  $a_0$  is the initial semi-major axis of the CO binary. The radius  $r_t$  is an approximation to the distance where within the tidal forces by the SMBH exceed the self-binding energy of the binary. The exact distance will depend on the orbital parameters and orientation of the binary (Hamilton & Burns 1991, 1992). One of the objectives of our study is to provide a statistical estimate of the tidal radius from our set of encounters.

As mentioned before, the effect of the encounter is a redistribution of energy and angular momentum in the system. As a consequence, orbital parameters in the CO binary, such as eccentricity and semi-major axis are affected. Regarding eccentricity, Heggie & Rasio (1996) provided an analytic estimate of this perturbation for a circular binary system in parabolic orbit around a third body. For the case of  $M_\bullet \gg M_b$ , the perturbation reads

$$\delta e = 3\sqrt{2\pi} \left(\frac{M_b}{M_\bullet}\right)^{1/4} \left(\frac{2r_p}{a_0}\right)^{3/4} \times \exp\left[-\frac{2}{3} \left(\frac{2M_b}{M_\bullet}\right)^{1/2} \left(\frac{r_p}{a_0}\right)^{3/2}\right] \mathcal{F}(\iota, \phi) \quad (12)$$

where

$$\mathcal{F}(\iota, \phi) = \cos^2 \frac{\iota}{2} \left[ \cos^4 \frac{\iota}{2} + \frac{4}{9} \sin^4 \frac{\iota}{2} + \frac{4}{3} \cos^2 \frac{\iota}{2} \sin^2 \frac{\iota}{2} \cos \phi^{1/2} \right]$$

with  $\iota$  the inclination of the CO binary relative to the orbit around the hole, and  $\phi$  depending on the initial phase of the binary and the longitude of the ascending node. Inserting the definition of tidal radius, Eq. 12 becomes

$$\delta e = 6\sqrt{\pi} 2^{1/4} \beta^{-3/4} \exp\left[-\frac{2\sqrt{2}}{3} \beta^{-3/2}\right] \mathcal{F}(\iota, \phi) \quad (13)$$

This expression will be compared against our simulation results in section 6.1. Since  $\delta e$  vanishes as inclination  $\iota \rightarrow \pi$  and  $\beta \rightarrow 0$ , we expect to see stronger agreement between simulation results and Eq. 13 for the low inclination and large pericenter encounters.

### 3. BINARY ENCOUNTER SETUP

The CO binary is injected in a parabolic orbit around the SMBH. The integration runs until either the binary is tidally disrupted by the SMBH and an amount of time equal to the initial time passes, or the center of mass of the binary has reached a true anomaly of  $\Theta = -\Theta_0$ , where  $\Theta_0 < 0$  is the initial true anomaly of the orbit of the binary's center of mass about the SMBH.

The following parameters in the three-body system are kept fixed: SMBH mass ( $M_\bullet = 10^6 M_\odot$ ), CO binary masses ( $m_1 = m_2 = m = 10 M_\odot$ ), initial binary eccentricity ( $e_0 = 0$ ), and initial binary semi-major axis ( $a_0 = 10 R_\odot = 0.047 \text{ AU}$ ). With these parameters, the CO binary has a period

$$P_{b,0} = \frac{2\pi a_0^{3/2}}{\sqrt{GM_b}} = 7.16 \times 10^4 \text{ s} \left(\frac{a_0}{10 R_\odot}\right)^{3/2} \left(\frac{M_b}{20 M_\odot}\right)^{-1/2}, \quad (14)$$

and tidal radius of the three-body system is

$$r_t = 173 r_g M_6^{-2/3} \left(\frac{M_b}{20 M_\odot}\right)^{-1/3} \left(\frac{a_0}{10 R_\odot}\right) = 1.73 \text{ AU} M_6^{1/3} \left(\frac{M_b}{20 M_\odot}\right)^{-1/3} \left(\frac{a_0}{0.047 \text{ AU}}\right). \quad (15)$$

where  $M_6 \equiv M_\bullet/10^6 M_\odot$  and  $r_g = GM_\bullet/c^2$  is the gravitational radius.

The parameters we vary are the CO binary orbital inclination  $\iota$ , the initial longitude of the ascending node  $\Omega_0$ , the binary initial phase  $\theta_0$ , and the pericentric distance  $r_p$  via the penetration factor  $\beta$ . Thus, our simulations of CO binary encounters with a SMBH span a four-dimensional parameter space  $\{\beta, \iota, \Omega_0, \theta_0\}$ . We sample this parameter space with random values taking uniform distributions in  $\beta^{-1} \in [0.35, 5]$ ,  $\cos \iota \in [-1, 1]$ , and  $\Omega_0 \in [0, 2\pi]$ . For the phase  $\theta_0$ , we take 200 evenly spaced values between 0 and  $2\pi$ . The distribution in  $\beta^{-1}$  implies that the values of the pericentric distance are uniformly distributed in  $r_t \in [0.865, 8.65] \text{ AU}$ . Furthermore, since the duration of the encounter is of order

$$T_p = \frac{2\pi r_p^{3/2}}{\sqrt{GM_\bullet}} = \beta^{-3/2} P_{b,0}, \quad (16)$$

the range of parameters we consider for  $\beta^{-1}$  imply that  $T_p \in [0.1, 3] P_{b,0}$ . Moreover, in the nomenclature of Heggie, our binary system is “soft” since

$$\frac{1}{2} M_b V_p^2 \gg -E_{b,0} \quad (17)$$

which can be seen from

$$\begin{aligned} \frac{1}{2} M_b V_p^2 &= \frac{GM_b M_\bullet}{r_p} = \frac{GM_b^2}{a_0} \left(\frac{M_\bullet}{M_b}\right)^{2/3} \beta \\ &\gg \frac{GM_b^2}{4a_0} = -E_{b,0}. \end{aligned} \quad (18)$$

Also, since  $r_t \sim 173 r_g$ , even for the deepest penetration encounters with  $\beta = 2$ , the pericentric distance will be  $r_p = 87 r_g$ . Therefore, it is perfectly safe to ignore general relativistic effects in all our encounters. Similarly, given that at pericentric passage

$$\frac{v^2}{c^2} \sim \frac{GM_\bullet}{c^2 r_p} \sim \frac{1}{87}, \quad (19)$$

post-Newtonian corrections to the orbital motion of the binary are at the level of a percent and thus will be ignored. However, in analyzing the the aftermath of an

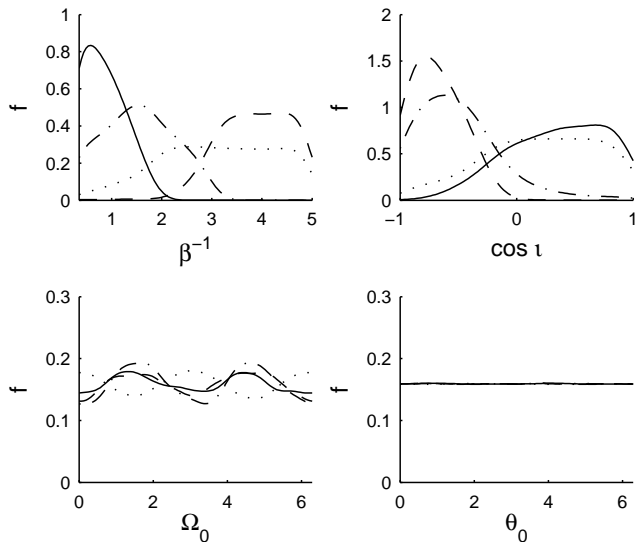


FIG. 1.— KDE probability distribution function  $f$  as computed from Eq. 21 for each of the  $\{\beta, \iota, \Omega_0, \theta_0\}$  parameters. The pdf  $f$  represents the probability that a binary with a particular end-state began with a particular value of a certain parameter. The lines-class correspondence is: solid denotes class DB, dot-dash class long BEMRI, dash class short BEMRI, and fine dash class SU.

encounter, we will take into account the Peters lifetime  $\tau_{gw}$  of the binary, if survived, or if the EMRI if the binary is disrupted. For the CO binary systems that we consider, the Peters lifetime due to the emission of GWs in the absence of the SMBH is (Peters 1964)

$$\tau_{gw,0} = 0.95 \times 10^8 \text{ yr} \left( \frac{a_0}{10 R_\odot} \right)^4 \left( \frac{M_b}{20 M_\odot} \right)^{-3}. \quad (20)$$

The present study consists of  $N_c \approx 13$  million individual simulations, resulting in: 2.1 million simulations of DB type encounters, 1.7 million yielding long BEMRI, 2 million producing short BEMRIs and 7.1 million of the SU type. We integrate the Newtonian equations of motion for the three-body system using Burlish-Stoer extrapolation with a leap-frog integrator as described in Mikkola & Tanikawa (1999). We increase the accuracy of the integration by the use of the CHAIN concept ala Mikkola & Aarseth (1993). The coordinate system used for the numerical integration are barycentric coordinates with the three body center of mass at the origin. The orbital angular momentum of the CO binary–SMBH system is aligned with the  $z$ -axis. That is, the plane of the CO binary center of mass orbiting the SMBH is the  $xy$ -plane. We inject the CO binary in the first quadrant ( $x, y > 0$ ) at a distance  $200 r_p$  and orient the orbit of the CO binary about SMBH such that pericentric distance  $r_p$  occurs along the  $x$ -axis, specifically at  $y = 0$  and  $x < 0$ . Conservation of energy and angular momentum is checked at every time step, and simulations are halted and rejected if either quantity deviates from the initial value by one part in  $10^6$ .

#### 4. PARAMETER PROBABILITY DISTRIBUTIONS AND TIDAL RADIUS

As already mentioned, we have classified the encounters into four types: DBs, long and short BEMRIs and SUs. Next, for each of these outcome types, we estimate the probability distribution as a function of the varying

parameters  $\{\beta, \iota, \Omega_0, \theta_0\}$ . For example,  $f(\beta^{-1}|DB)$  is the probability distribution function for the parameter  $\beta^{-1}$  for disrupted binaries, i.e. the probability that a disrupted binary had a particular value of  $\beta^{-1}$  (solid curve in upper left panel of Figure 1). We use for this purpose the technique of kernel density estimation (KDE). KDE is a non-parametric method for estimating probability densities in which a kernel function  $K$  is convolved with a collection of Dirac delta functions. KDE asymptotically converges to the true distribution faster than histograms (Scott 1979). The KDE probability distribution  $f$  of a parameter  $x$  is computed from

$$f(x) = \frac{1}{N} \sum_{n=0}^N K(x) * \delta(x - x_n) = \frac{1}{N} \sum_{n=0}^N K(x - x_n) \quad (21)$$

where  $N$  is the number of data points in the sample. We use a Gaussian kernel  $K(x) = (2\pi h^2)^{-1/2} \exp[-x^2/(2h^2)]$  with a variance of  $h^2 = [\text{parameter range}]/100$ , chosen to produce distributions that retain structure while not being over-smoothed. Figure 1 shows the resulting normalized KDE probability distributions  $f$  for each of the  $\{\beta, \iota, \Omega_0, \theta_0\}$  parameters obtained from Eq. 21.

We can draw from these probability distributions several conclusions about the nature of the end-state of the binary relative to the input parameters, as well as the predictive power of the individual parameters. It is clear from the panel of the  $\beta^{-1}$  probability distribution (top left panel in Figure 1) that the encounters yielding binary disruption (i.e. DB-type, black, dot-dash line) occur primarily for small values of  $\beta^{-1}$  or large penetration factors  $\beta$ . This should be obvious: closer passes translates into stronger tidal forces and higher likelihood of disruption. Additionally, regarding the parameter  $\iota$ , prograde binaries (defined here as those with inclination  $\iota < \pi/2$ ) are more probable to disrupt than retrograde binaries (those with  $\iota > \pi/2$ ). This is so because, in general, retrograde binaries are more likely to survive and become bound to the SMBH, implying that while the BH orbit loses energy, the surviving retrograde binaries must gain an equal amount energy, though not generally enough to disrupt.

Notice that the probability distribution for the initial orbital phase  $\theta_0$  is flat. That is, the value of  $\theta_0$  does not play a role on the outcome of the encounter. The distributions in Figure 2 are over all the simulations in the parameter space. The flat distribution in  $\theta_0$  illustrates that there is no strong correlation between  $\theta_0$  and disruption across the entire parameter space of interest; the combination of other parameters has far greater influence. Clearly if all parameters except  $\theta_0$  were fixed, some binaries would be disrupted, but there is no consistent trend. Also interesting is that the probability of longitude of the ascending node  $\Omega_0$  is relatively flat. Therefore, we will focus our attention on the parameters  $\beta$  and  $\iota$  since they have the largest effect on the binary end state.

The fact that  $\beta$  and  $\iota$  are the most relevant parameters can also be seen in Figure 2 where we show the fraction of surviving binaries for each parameter. Consistent with Figure 1, the top panels in Figure 2 show that the survival probability depends more strongly on  $\beta^{-1}$  and  $\iota$ . The top right panel shows again that prograde ( $\iota < \pi/2$ ) binaries in general more likely to be disrupted than ret-

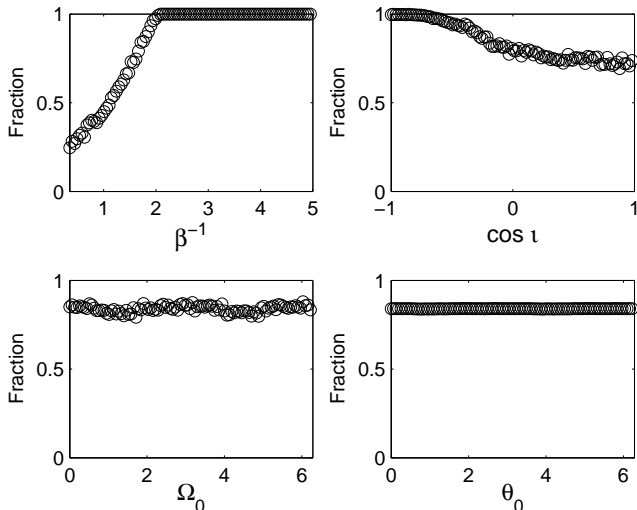


FIG. 2.— Fraction of surviving binaries as a function of each in parameter for each parameter  $\{\beta, \iota, \Omega_0, \theta_0\}$ .

rograde ( $\iota > \pi/2$ ) binaries. Similarly, it is clear from the top left panel that the probability of disruption goes to zero for  $\beta^{-1} \gtrsim 2.1$ . Also consistent with Figure 1, the bottom panels in Figure 2 show that  $\Omega_0$  and  $\theta_0$  have a very weak influence on the survival ratio. Therefore, we can assume with confidence that for practical purposes the parameter space is two-dimensional, namely  $\{\beta, \iota\}$ .

The dependence of the binary survival on  $\iota$  implies that the tidal radius does not only depend on  $\beta$  but also on the inclination of the binary. This is not surprising because the forces from the SMBH responsible for disrupting the binary are those projected along the semi-major axis of the binary. Figure 3 depicts a two-dimensional histogram of tidal disruptions as a function of  $\cos \iota$  and  $\beta^{-1}$ . The solid line is the condition obtained by setting in Eq. 12 the eccentricity perturbation to  $\delta e = 1$  with  $\phi = 0$  to maximize the effect. Namely,

$$\mathcal{F}^{-1}(\iota, 0) = 6\sqrt{\pi} 2^{1/4} \beta^{-3/4} \exp\left[-\frac{2\sqrt{2}}{3}\beta^{-3/2}\right] \quad (22)$$

Notice that this analytic approximation bounds the region containing disruptions well for  $\beta^{-1} \gtrsim 1$ , but does not do so well for  $\beta^{-1} < 1$ , where the deepest penetration encounters are located.

## 5. DISRUPTED BINARIES

As stated in the introduction, CO binaries disrupted by the SMBH are of interest as both sources of EMRIs and HVSs. In this section, we investigate the channels for EMRI formation and use previous HVS results as a check for our simulation accuracy.

We recall that after a binary is disrupted, the total energy of the system is approximately given by  $E = E_1 + E_2 = E_{b,0}$ , where  $E_{b,0}$  is the initial binding energy of the CO binary and

$$E_i = \frac{1}{2}m_i v_i^2 - \frac{Gm_i M_\bullet}{r_i}, \quad (23)$$

with  $i = 1, 2$ .

Figure 4 shows the combined histograms of the normalized energies  $E_1/|E_{b,0}|$  and  $E_2/|E_{b,0}|$  (top panel) and the

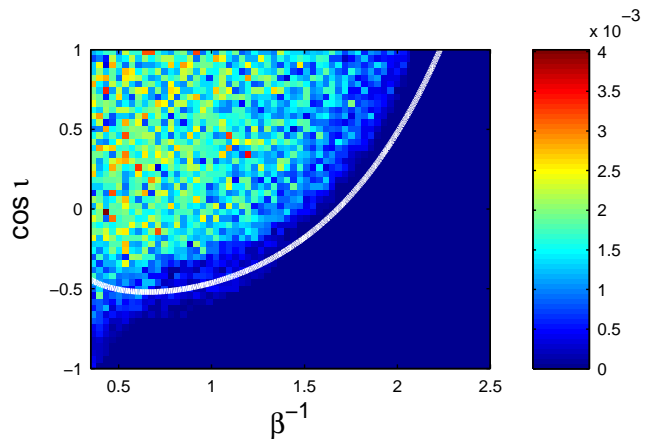


FIG. 3.— 2D histogram of disruptions vs.  $\beta^{-1}$  and  $\cos \iota$ , shown as fraction of total disruptions. The white line denotes Eq. 22.

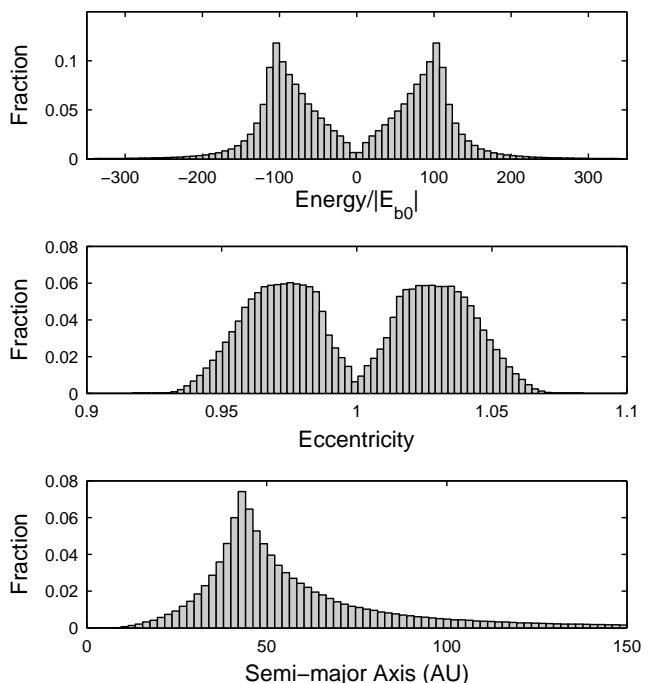


FIG. 4.— Top panel: Histogram of the binding energy  $E_i$  from Eq. 25 normalized to the initial binding energy of the binary  $E_{b,0}$ . Middle panel: Histogram of the corresponding eccentricity. Bottom Panel: Histogram of resulting EMRI semi-major axis. Histograms shown as fraction of total disruptions.

corresponding eccentricities (bottom panel). The symmetry of the histograms gives the impression when a binary is disrupted the outcome is invariable one component bound to the SMBH, i.e. an EMRI, and the other component unbound to the hole, namely a HVS. This is indeed the case for most of the disruptions ( $\sim 99.9967\%$ ). However, since  $E_1 + E_2 = E_{b,0} < 0$ , there are cases, although rare ( $\sim 0.0033\%$ ), for which both  $E_1 < 0$  and  $E_2 < 0$ , and the outcome is two EMRIs. Moreover, notice from the bottom panel in Figure 4 that the average eccentricity for the bound (unbound) component of the disrupted binary is  $e_- \approx 0.97$  ( $e_+ \approx 1.3$ ). This can be

understood from the definition of eccentricity

$$e_{\pm}^2 = 1 + \frac{2 E_{\pm} L_{\pm}^2}{G^2 m_{\pm}^3 M_{\bullet}^2}, \quad (24)$$

where we approximate

$$E_{\pm} \approx \pm G M_{\bullet} m_{\pm} a_0 r_p^{-2} \quad (25)$$

and

$$L_{\pm}^2 \approx L_{\text{cm}}^2 = 2 G M_{\bullet} m_{\pm}^2 r_p. \quad (26)$$

Thus,

$$\begin{aligned} e_{\pm}^2 - 1 &= \pm 4 \frac{a_0}{r_p} = \pm 4 \beta \frac{a_0}{r_t} = \pm 4 \beta \left( \frac{M_b}{M_{\bullet}} \right)^{1/3} \\ e_{\pm} &\approx 1 \pm 0.05 \beta \left( \frac{M_b}{20 M_{\odot}} \right)^{1/3} M_6^{-1/3}. \end{aligned} \quad (27)$$

Furthermore, from Eq. 25 and  $E_{b,0} = |G M_b^2 / (4 a_0)|$ , we have that

$$\frac{E_{\pm}}{|E_{b,0}|} \approx \pm 74 \beta^2 M_6^{1/3} \left( \frac{M_b}{20 M_{\odot}} \right)^{-1/3}, \quad (28)$$

consistent with the histograms in the top panel of Figure 4.

### 5.1. Ejected Hyper-velocity Stars

Hypervelocity stars are stars with velocities of the order of hundreds or thousands of  $\text{km s}^{-1}$ , which may exceed the escape velocity of our galaxy. These stars were predicted by Hills (1988) as the result of binary disruption in the galactic center, and discovered observationally nearly two decades later (Brown et al. 2005; Edelmann et al. 2005).

The production of HVS from the tidal disruption of binary systems by a SMBH has been discussed by Hills (1988); Yu & Tremaine (2003); Antonini et al. (2010); Bromley et al. (2006). Our study is consistent with those results. From Eq. 25 and  $E_i = m_i v_{\infty}^2 / 2$ , one has that

$$\begin{aligned} v_{\infty}^2 &\approx 2 G M_{\bullet} a_0 r_p^{-2} \\ &\approx 2 G \beta^2 M_{\bullet} a_0 r_t^{-2} \\ &\approx 2 G \beta^2 M_{\bullet}^{1/3} a_0^{-1} M_b^{2/3}, \end{aligned} \quad (29)$$

which yields the following asymptotic velocity approximation of a HVS

$$\begin{aligned} v_{\infty} &\approx 5,312 \text{ km/s} \cdot \beta \cdot M_6^{1/6} \\ &\times \left( \frac{a_0}{0.047 \text{ AU}} \right)^{-1/2} \left( \frac{M_b}{20 M_{\odot}} \right)^{1/3}. \end{aligned} \quad (30)$$

Rescaled to our case, the numerical study by Bromley et al. (2006) found that

$$\begin{aligned} v_{\infty} &\approx 4,468 \text{ km/s} \cdot g(D) \cdot M_6^{1/6} \\ &\times \left( \frac{a_0}{0.047 \text{ AU}} \right)^{-1/2} \left( \frac{M_b}{20 M_{\odot}} \right)^{1/3} \end{aligned} \quad (31)$$

where

$$\begin{aligned} g(D) &= 0.774 + 0.0204 D - 6.23 \times 10^{-4} D^2 \\ &+ 7.62 \times 10^{-6} D^3 - 4.24 \times 10^{-8} D^4 \\ &+ 8.62 \times 10^{-11} D^5. \end{aligned} \quad (32)$$

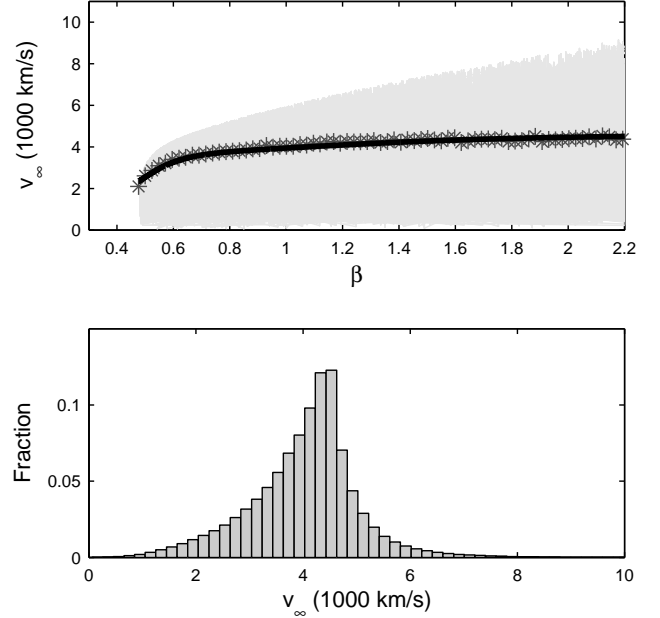


FIG. 5.— Top panel: Grey dots denoted the ejection velocity  $v_{\infty}$  as a function of  $\beta$  for all the unbound stars from disrupted binaries. Stars show the averages over 100 evenly spaced intervals in  $\beta$ . Solid line shows the model prediction from Eq. 31. Bottom panel: distribution of  $v_{\infty}$  for all ejected components.

with  $D = 79.37 \beta^{-1}$ .

In the top panel in Figure 5 we show with grey dots the ejection velocity  $v_{\infty}$  as a function of  $\beta^{-1}$  for all the unbound stars from disrupted binaries. In the same panel, stars show the averages over 100  $\beta$  bins. The solid line shows the model prediction from Eq. 31. The agreement of our average velocities with those from Bromley et al. (2006) is evident. However, it should be noted that the range of possible velocities can vary significantly from this average, with the largest values roughly double the analytic prediction and nearly 59% of ejections in our simulations exceeding the predicted value.

### 5.2. Extreme-Mass-Ratio Inspirals

The traditional formation channel of an EMRI is when two-body relaxation not only bounds a star to a SMBH but also brings it into the GW-emission inspiraling regime (Amaro-Seoane et al. 2007). The pericentric distance to capture a star bound to a SMBH with semi-major axis  $a_c$  and form an EMRI is

$$r_c \approx 3 r_g M_6^{-4/7} \left( \frac{m}{10 M_{\odot}} \right)^{2/7} \left( \frac{a_c}{0.05 \text{ pc}} \right)^{2/7}. \quad (33)$$

Since the star needs to penetrate so deeply into the neighborhood of the SMBH, despite circularization from GW emission, the EMRI arrives to merger with significant eccentricity,  $e \sim 0.5 - 0.9$ .

The disruption of a binary by a SMBH provides an alternative channel since the disruption will always leave at least one component bound to the SMBH. The capture distance in this situation is much larger. It is not  $r_c$  but the tidal radius  $r_t \sim 173 r_g$  (see Eq. 15). Being bound to the SMBH does not necessarily translate into becoming an EMRI. The condition for a star to qualify as an EMRI is that the timescale  $\tau_{\text{gw}}$  for its orbital

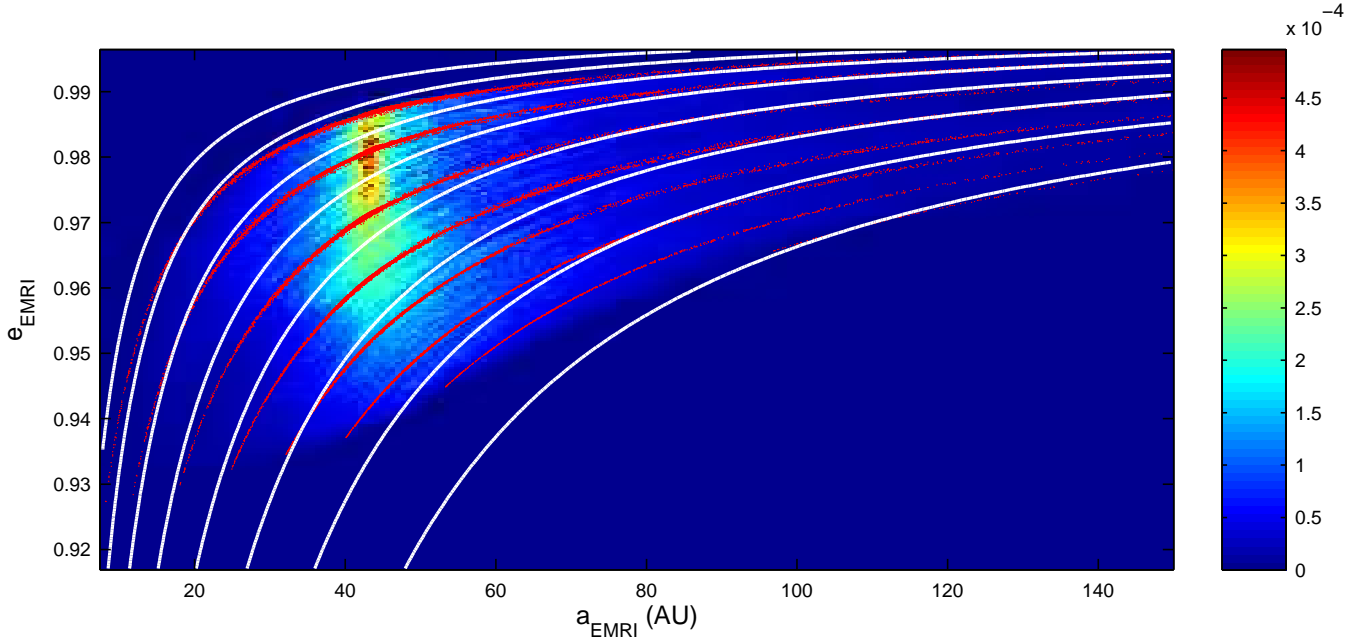


FIG. 6.— 2D histogram of potential EMRI candidates as a function of eccentricity  $e_i$  and semi-major axis  $a_i$ , shown as fraction of total disruptions. White lines are lines of constant Peters lifetime with values  $\tau_{\text{gw}} = 10^\alpha$  years, where from left to right  $\alpha = 5.0, 5.5, 6.0, 6.5, 7.0, 7.5, 8.0$  and  $8.5$ , respectively. Red lines show lines of constant  $\beta^{-1}$  with  $\beta^{-1} = 0.35, 0.5, 0.75, 1.0, 1.25, 1.5, 1.75,$  and  $2.0$  from left to right.

decay by GW emission is sufficiently shorter than the relaxation time  $t_{\text{rlx}}$  of the stars in the galactic center (Amaro-Seoane et al. 2007):

$$t_{\text{rlx}} \approx 1.8 \times 10^8 \text{ yr} \left( \frac{\sigma}{100 \text{ km s}^{-1}} \right)^3 \times \left( \frac{10 M_\odot}{m} \right) \left( \frac{10^6 M_\odot \text{ pc}^{-3}}{\bar{m} n} \right) \quad (34)$$

where  $\sigma$  is the local velocity dispersion,  $n$  is the local number density of stars, and  $\bar{m}$  is the average stellar mass.

Figure 6 displays a 2D histogram of  $(a, e)$  for EMRI candidates from the disruption of binaries. White lines are lines of constant Peters lifetime with values  $\tau_{\text{gw}} = 10^\alpha$  years, where from left to right  $\alpha = 5.0, 5.5, 6.0, 6.5, 7.0, 7.5, 8.0$  and  $8.5$ , respectively. Red lines show lines of constant  $\beta^{-1}$  with  $\beta^{-1} = 0.35, 0.5, 0.75, 1.0, 1.25, 1.5, 1.75,$  and  $2.0$  from left to right. It is clear from this histogram that most of the candidates qualify as EMRIs since  $\tau_{\text{gw}} \ll t_{\text{rlx}} \approx 10^8 \text{ yr}$ . Also interesting is that the encounters with deepest penetration factors, i.e. small  $\beta^{-1}$ , yield EMRIs with larger eccentricity.

Our results are consistent with those from Miller et al. (2005) in the following respect. Because their “capture” radius is much larger than in the traditional scenario, i.e.  $r_t \sim 170 r_g$  instead of  $r_c \sim \text{few } r_g$ , the EMRI from binary disruptions will have circularized dramatically by the time they merger or they enter the sensitive band of a LISA-like detector. One can see this using Peters (1964)

$$a(e) = \frac{c_0 e^{12/19}}{(1 - e^2)} \left( 1 + \frac{121}{304} e^2 \right)^{870/2299} \quad (35)$$

with  $c_0$  determined by the initial condition  $a = a_0$  when  $e = e_0$ . From Figure 6, we have that at “birth” the EMRI

will have a typical eccentricities of  $e_0 \approx 0.97$  and semi-major axis  $a_0 \approx 45 \text{ AU}$ ; thus,  $c_0 \approx 2.3 \text{ AU}$  in Eq. 35. For a space-based interferometer like LISA, the low end of the sensitivity window is  $f_{\text{gw}} \sim 10^{-4} \text{ Hz}$ . If we approximate  $f_{\text{gw}} \approx 2f$  with  $f^{-1} = P = 2\pi a^{3/2}/\sqrt{GM_\bullet}$  the Keplerian orbital period, we have that when the EMRI enters the sensitivity band of a LISA-like detector it has a semi-major axis of

$$a \lesssim 74 r_g \left( \frac{f_{\text{gw}}}{10^{-4} \text{ Hz}} \right)^{-2/3} M_6^{-2/3}. \quad (36)$$

From Eq. 35, one has that the corresponding eccentricity is  $e \lesssim 0.15$ . By the time the EMRI merges, i.e.  $a \sim r_g$ , it will have eccentricity  $e \sim 10^{-4}$  and emit GWs at dominant frequencies of  $f_{\text{gw}} \approx 60 \text{ mHz}$ . This is clear from Figure 7 where we plot the eccentricity of the EMRIs as a function of the GW frequency  $f_{\text{gw}}$ . We approximate  $f_{\text{gw}} \approx 2f$  with  $f^{-1} = P = 2\pi a^{3/2}/\sqrt{GM_\bullet}$  the Keplerian orbital period and  $a$  from (Peters 1964). Figure 7 shows that in the sensitive LISA band ( $0.1 \text{ mHz} \lesssim f_{\text{GW}} \lesssim 100 \text{ mHz}$ ), EMRIs can have average eccentricity  $\bar{e} \leq 0.1$ . At the most sensitive frequencies, however, at  $f_{\text{GW}} \lesssim 10 \text{ mHz}$ , these EMRIs will have typical eccentricities  $e < 0.01$ , in agreement with Miller et al. (2005).

## 6. SURVIVING BINARIES

We now turn the attention to the population of binaries that survive the encounter with the SMBH. These binaries make up the majority of the encounters we simulated given the range of values of  $\beta$  we considered. In these scenarios, the energy exchange is simpler: energy is either drained from the orbit of the binary around the BH and donated to the CO binary orbit, or vice versa (see Eq. 6). In general terms, we expect the binary to soften and become bound to the SMBH or to tighten and

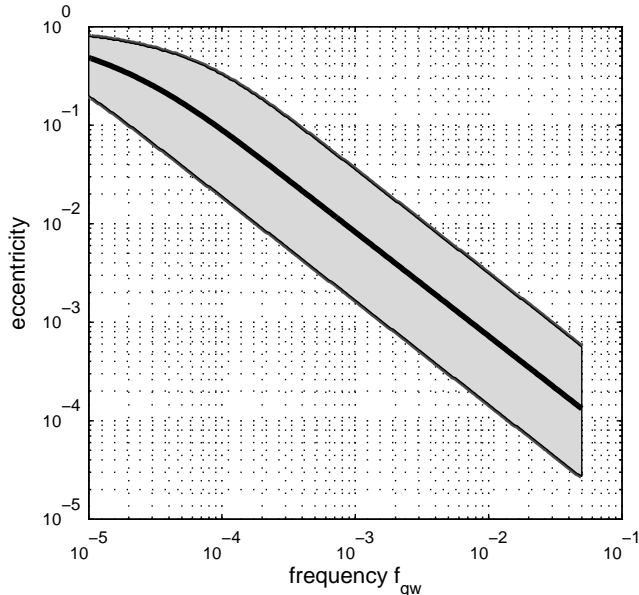


FIG. 7.— EMRI eccentricity at fundamental frequency  $f_{\text{gw}}$ . Eccentricity for individual EMRIs are shown in gray, average shown in black.

remain unbound. Specifically, the surviving binaries will belong to one of the following types: binaries bound to the SMBH with a Peters lifetime  $\tau_{\text{gw}}$  longer than their orbital period  $P_{\bullet}$  about the hole (i.e. long BEMRIs); binaries also bound to the SMBH but that merge before completing an orbit around the hole,  $\tau_{\text{gw}} < P_{\bullet}$  (i.e. short BEMRIs); and binaries that are unbound from the SMBH. We will analyse the distributions of orbital parameters (eccentricity and semi-major axis) of the surviving binaries, with the goal of determining the net change to merger lifetime and whether this leads to detectable changes in the CBC rate observed by detectors such as LIGO. But before doing so, we will briefly revisit the effect of  $\theta_0$  and  $\Omega_0$ .

In Section 4, we estimated probability distributions of the parameters  $\{\beta, \iota, \theta_0, \Omega_0\}$  for each of the encounter types. We observed that the distributions for the phase of the binary  $\theta_0$  and the longitude of the ascending node  $\Omega_0$  are to a good approximation flat. Thus, the parameters  $\beta$  and  $\iota$  have a more dominant role on the outcome. This does not mean that choices of  $\theta_0$  and  $\Omega_0$  do not influence the end state. Figure 8 displays the eccentricity of the CO binary after the encounter with the SMBH as a function of  $\theta_0$ . In the upper panel, we show with dots cases with parameters  $(\beta^{-1}, \iota, \Omega_0) = (0.77, 123^\circ, 46^\circ)$ , squares with  $(1.9, 101^\circ, 312^\circ)$ , and diamonds with  $(4.6, 49^\circ, 152^\circ)$ . Points where the curve jumps above 1 indicate disrupted binaries. Notice as expected that as the penetration factor increase, so the eccentricity gained by the binary as well as its dependence of the initial binary phase. In the lower panel in Figure 8 we show with circles parameters  $(\beta^{-1}, \iota, \Omega_0) = (0.57, 177^\circ, 255^\circ)$  and with squares have  $(1.7, 79^\circ, 308^\circ)$ . Notice that binaries making a closer pass (circles) generally suffers a reduced perturbation to eccentricity due to the nearly retrograde orbit.

### 6.1. Post-Encounter Binary Eccentricity

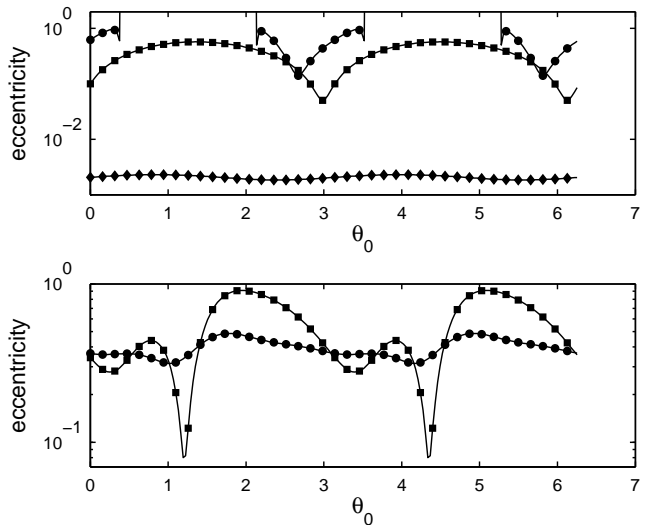


FIG. 8.— Resulting eccentricity of surviving binaries as a function of  $\theta_0$ . Upper panel: the dots show cases with parameters  $(\beta^{-1}, \iota, \Omega_0) = (0.77, 123^\circ, 46^\circ)$ , squares with  $(1.9, 101^\circ, 312^\circ)$ , and diamonds with  $(4.6, 49^\circ, 152^\circ)$ . Points where the curve jumps above 1 indicate disrupted binaries. Lower panel: dots with parameters  $(\beta^{-1}, \iota, \Omega_0) = (0.57, 177^\circ, 255^\circ)$ , and squares with  $(1.7, 79^\circ, 308^\circ)$ .

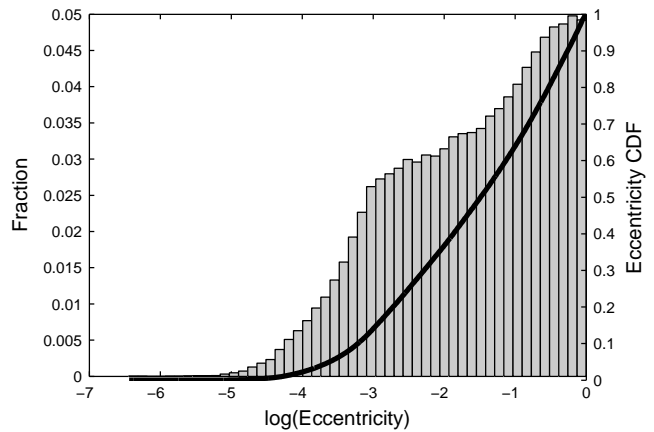


FIG. 9.— Fraction of surviving binaries as a function of post-encounter eccentricity as well as with a solid line the cumulative distribution function (CDF) of the eccentricity values.

In Figure 9, we show the fraction of surviving binaries as a function of post-encounter eccentricity as well as the cumulative distribution function (CDF) of the eccentricity values. Note that the majority of the surviving binaries are relatively unperturbed in eccentricity, with the 65% quantile lying at approximately  $e \approx 0.109$  and the 90% quantile at  $e \approx 0.553$ .

Figure 10 show how the post-encounter eccentricity depends on  $\beta^{-1}$  and  $\iota$ . The surviving binary acquires eccentricity for larger penetration factors (smaller  $\beta^{-1}$ ) and prograde orbits ( $\cos \iota > 0$ ). Contours of constant  $\log e = -5.5, -5.0, -4.5, \dots, 0$  from right to left are shown in white. Black lines are the corresponding estimates obtained from Eq. 13 averaged over  $\phi$ . Notice that the contour for  $\log e = 0$  is not present for the simulation data. All simulation values have been averaged over  $\theta_0$ . As expected, we see better agreement between the prediction from Eq. 13 and simulation results for large  $\beta^{-1}$

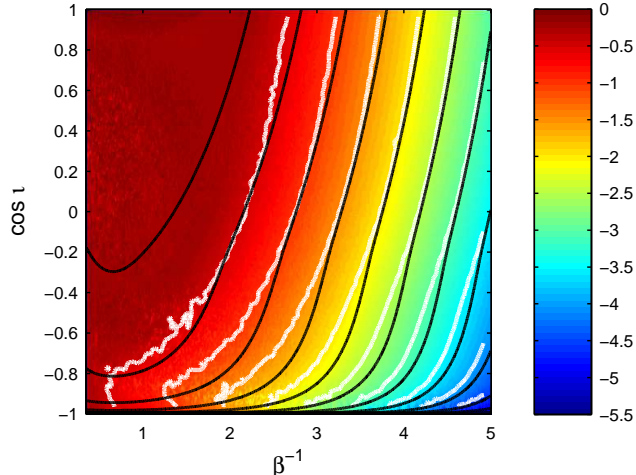


FIG. 10.— Resulting eccentricity  $\log e$  for surviving binaries plotted as an intensity map vs.  $\beta^{-1}$  and  $i$ . Contours of constant  $\log e = -5.5, -5.0, -4.5, \dots, 0$  are shown from right to left in white and for the analytic estimate from Eq. 13 in black.

and small  $i$  since that is the regime where Eq. 13 was derived. The small overestimation of the prediction at small inclination is consistent with what was found in Heggie & Rasio (1996) for an equal mass binary.

Finally, Figure 11 shows gray scale maps of the post-encounter  $\log e$  against pairs of parameters  $\beta^{-1}$ ,  $i$ , and  $\Omega_0$ , averaged over  $\theta_0$ . Noticeable are the different effects of the input parameters. As  $\beta^{-1}$  increases, the final eccentricity decreases toward zero, however even binaries with  $\beta^{-1} = 3$  can receive a non-negligible amount of eccentricity,  $e \sim 0.2$ , after the encounter. Inclination plays a smaller but important role in determining the allowable range of final eccentricities, with eccentricity decreasing as the binary orbit approaches retrograde with respect to the SMBH orbit. As stated before, the longitude of the ascending node  $\Omega_0$  plays no predictable role in the perturbed eccentricity.

### 6.2. Post-Encounter Binary Semi-major Axis

Semi-major axis of the surviving binaries is shown as a histogram in Figure 12. The semi-major axis has been normalized to its initial value. It is clear that the semi-major axis is generally not perturbed to a strong degree, with the overall mean being  $\langle a/a_0 \rangle = 1.03$ . If the sample size is restricted to binaries with final semi-major axes in the range  $0.5 < a/a_0 < 1.5$ , which accounts for  $> 97\%$  of the data and removes the outliers, then the mean is  $\langle a/a_0 \rangle = 0.988$  and standard deviation of 0.084.

Figure 13 is similar to Figure 11 but for  $a/a_0$ . It can be seen here that for  $\beta^{-1} < 2$  the binary can suffer a large change to the semi-major axis, while above this value the change is small. Inclination has the general effect of tightening the binary for  $i < \pi/2$ , and loosening it for  $i > \pi/2$ . There is some variation in the extent of semi-major axis perturbation as a function of  $\Omega_0$ , particularly when the inclination is around  $i \approx \pi/2$  or at low values of  $\beta^{-1}$ , with minimum change at  $\Omega_0 \approx 0$  or  $\pi$ .

Since the binding energy of the binary is related to the semi-major axis  $E_b \propto -a^{-1}$ , one can from Figure 13 identify regions of parameter space where the binding energy of the binary increases or decreases. Furthermore, given

that  $E = E_{cm} + E_b = E_{b,0} < 0$ , an increase in binary energy  $E_b$  must be compensated by a decrease in the BH orbit energy  $E_{cm}$ , resulting in capture of the binary. Therefore the points in Figure 13 where  $a/a_0 > 1$  correspond to binaries which become bound, while  $a/a_0 < 1$  indicates binaries that remain unbound.

## 7. PETERS LIFETIME AND CBC RATES

As mentioned before, the Peters lifetime is an estimate of the time that a binary system with eccentricity  $e$  and semi-major axis  $a$  takes to merge as it loses energy due to emission of GWs (Peters 1964). As presented in Equation 20, the CO binary system in our study, with initial semi-major-axis  $a_0 = 10 R_\odot$  and vanishing eccentricity (i.e. circular orbit), has a Peters lifetime of  $\tau_{gw,0} \approx 10^8$  years. Figure 14 shows the Peters lifetime  $\tau_{gw}$  normalized to  $\tau_{gw,0}$  for all of the surviving binaries. Notice the similarity of the maps with those for the semi-major axis in Figure 12.

Unbound binaries that survive the encounter with the SMBH, what we call SU binaries, could in principle have a shorter ( $\tau_{gw} < \tau_{gw,0}$ ) or longer ( $\tau_{gw} > \tau_{gw,0}$ ) Peters lifetime. The last situation, however, is not possible given our initial setup. An unbound binary requires increasing the energy of its center of mass  $E_{cm}$ . This will come at the expense of decreasing its binding energy  $E_b$  since  $E = E_{cm} + E_b = E_{b,0} < 0$ , which in turn requires decreasing its semi-major axis. A decrease in its semi-major axis translates into a shorter Peters lifetime. Thus, all of the unbound binaries in our study will have accelerated merger times due to the SMBH

We recall that a *short EMRI* is one for which  $\tau_{gw} < P_\bullet$ . That is, the binary is expected to merge before returning to the hole. On the other hand, a *long BEMRI* is one in which  $\tau_{gw} > P_\bullet$ . These BEMRIs have typically highly elliptical orbits with average eccentricity  $e_{cm} \approx 1 - 10^{-5}$  and long periods. Therefore,

$$\begin{aligned}
 P_\bullet &= \frac{2\pi a_{cm}^{3/2}}{\sqrt{GM_\bullet}} = \frac{2\pi r_p^{3/2}}{\sqrt{GM_\bullet}} (1 - e_{cm})^{-3/2} \\
 &= \beta^{-3/2} (1 - e_{cm})^{-3/2} \frac{2\pi r_t^{3/2}}{\sqrt{GM_\bullet}} \\
 &= \beta^{-3/2} (1 - e_{cm})^{-3/2} \frac{2\pi a_0^{3/2}}{\sqrt{GM_b}} \\
 &= 7.2 \times 10^4 \text{ yr } \beta^{-3/2} \\
 &\times \left( \frac{1 - e_{cm}}{10^{-5}} \right)^{-3/2} \left( \frac{P_{b,0}}{7.16 \times 10^4 \text{ s}} \right) \quad (37)
 \end{aligned}$$

The CO binary in a long BEMRI could potentially survive several orbits around the SMBH, with its orbit being perturbed by each passage. We will investigate the fate of BEMRI systems will be the focus of a future study.

Independently of being in an BEMRI or unbound, CO binaries that after an encounter with a SMBH are affected in such a way that  $\tau_{gw} < \tau_{gw,0}$  have particular interest. They could potentially increase the rates of CBC to be detected by LIGO. We construct a simple formula to obtain a first estimate of this effect as

$$\mathcal{E}_{CBC} = [\Gamma * f_b * N_G(D_h)] * (\mathcal{E}_T * f_L), \quad (38)$$

where  $\mathcal{E}_{CBC}$  is the enhancement to the current predicted

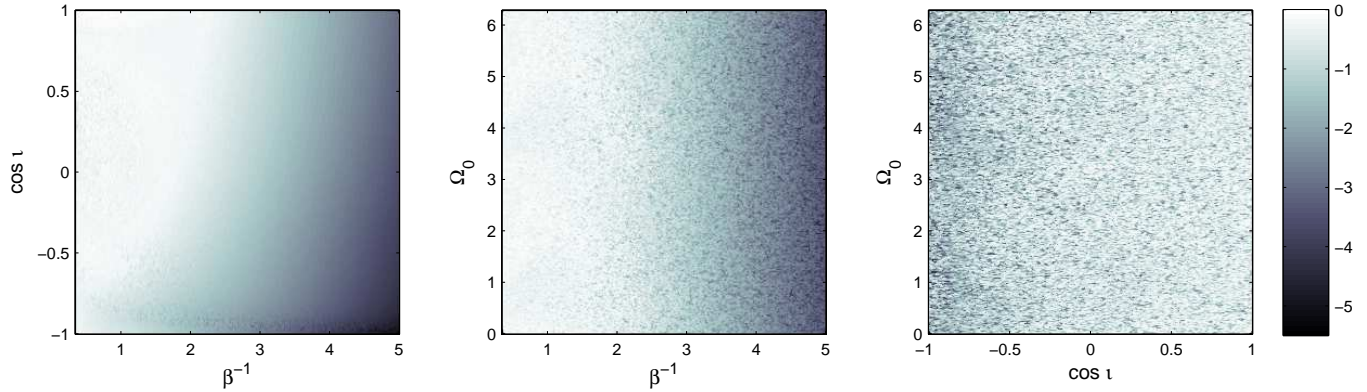


FIG. 11.— Gray scale maps of post-encounter  $\log e$  as a function of combinations of input parameters. All values have been averaged over  $\theta_0$ .

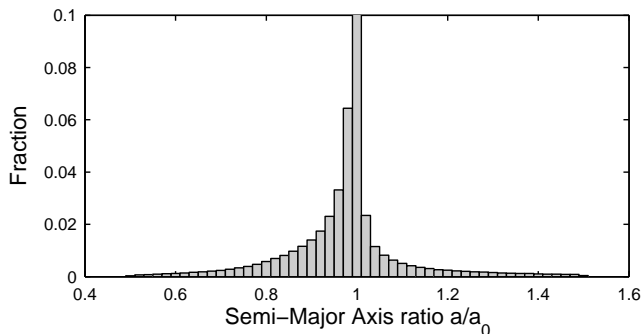


FIG. 12.— Histogram of the binary semi-major axis distribution after SMBH encounter. The horizontal axis has been stretched so that the few outliers did not dominate the plot scale, and the vertical axis has been truncated to show detail with the central bin having a true value of  $\sim 0.69$ . It is clear that the majority of encounter result in very small change in semi-major axis.

CBC rate  $R_{CBC}$ , i.e.,  $\hat{R}_{CBC} = R_{CBC} + \mathcal{E}_{CBC}$ . The first three terms in Eq. 38 are observational quantities taken from the literature.  $\Gamma$  is the estimated encounter rate of stellar mass objects / per SMBH per year,  $f_b$  is the binary fraction, and  $N_G(D_h)$  is the number of Milky Way equivalent galaxies (MWEGs) observable by a GW detector with horizon distance,  $D_h$ . The product of these factors is the rate of binary encounters with a SMBH in the observable volume of a GW detector.

The next two factors come from our simulation results. The single binary enhancement  $\mathcal{E}_\tau = (1 - \tilde{\tau}/\tau_0)$  is the percent difference between the old merger lifetime,  $\tau_0$ , and the mean new lifetime,  $\tilde{\tau}$ , and  $f_L$  is the fraction of binaries from our simulations that result in guaranteed LIGO sources after the SMBH encounter. Encounter rates in galaxies with a  $10^6 M_\odot$  SMBH, estimates for the single CO capture rate range from  $\Gamma \sim 5 \times 10^{-9} \text{ yr}^{-1} \text{ MWEG}^{-1}$  to as high as  $\Gamma \sim 10^{-6} \text{ yr}^{-1} \text{ MWEG}^{-1}$  (Hils & Bender (1995); Sigurdsson & Rees (1997); Ivanov (2002); Hopman & Alexander (2005); Merritt et al. (2011)); we use the higher side of these estimates,  $\Gamma = 10^{-7} \text{ yr}^{-1} \text{ MWEG}^{-1}$ , as the pericenter distances in our simulations reach much larger values than the single star capture radius. The binary fraction,  $f_b$ , near the galactic center is not a well determined value, however, in the absence of better knowledge, we take it to be roughly the same as the binary fraction of field

stars,  $f_b = 0.5$ . The number of MWEGs observable by aLIGO with a BH-BH merger horizon distance of  $D_h = 2187 \text{ Mpc}$  is given as (Abadie et al. (2010); Kalogera et al. (2001))

$$N_G = \frac{4}{3}\pi \left( \frac{D_h}{\text{Mpc}} \right)^3 \frac{0.0116}{(2.26)^3}, \quad (39)$$

which gives a value of  $N_G \approx 4.4 \times 10^7$  MWEGs.

From our simulation results, we find that binaries from the  $f_L$  categories have a mean Peters lifetime of  $\tilde{\tau} \approx 0.84\tau_0$  giving  $\mathcal{E}_T \approx 0.16$  and LIGO fraction  $f_L \approx 0.68$ . Combining these factors, we compute an estimated enhancement to the CBC rate of  $\mathcal{E}_{CBC} \approx 0.25 \text{ yr}^{-1}$ . The predicted rate of expected BH-BH mergers has been estimated to lie between  $0.4 \text{ MWEG}^{-1} \text{ Myr}^{-1} < \Gamma_{BH} < 30 \text{ MWEG}^{-1} \text{ Myr}^{-1}$  for realistic to optimistic scenarios Kalogera et al. (2007); Abadie et al. (2010). This corresponds to an estimated merger rate within the aLIGO volume of  $\sim 20 \text{ yr}^{-1} < \dot{N}_{BH} < 1300 \text{ yr}^{-1}$ , which our estimated rate enhancement  $\mathcal{E}_{CBC}$  may change by as much as  $\approx 1\%$ . This enhancement will likely be difficult to detect with small observation catalogs and given the uncertainty in the estimated merger rates, but could become noticeable over long observation times.

## 8. SUMMARY AND CONCLUSIONS

In this paper, we have presented the results of  $\sim 13$  million individual simulations of parabolic encounters between a CO binary and a galactic center SMBH while varying the orientation of the binary and its distance of closest approach to the SMBH.

Tidal disruption of the binary occurs with about 16% probability given the full range of parameters covered in this study. Consistent with previous work in this area, this sort of disruption can create HVS which can escape from the SMBH with high speed. We also explored disruption as a formation mechanism for EMRIs, which are of interest to space-based GW detection missions, and found that the EMRIs formed in this way will generally have very low eccentricity when they enter the LISA band. This work shows that considering the full range of possible orientations gives a broader range of formation eccentricities than previous estimates have predicted.

Surviving binaries can either become bound to the SMBH after the encounter and become a BEMRI or remain unbound from the hole. Among them, there is a

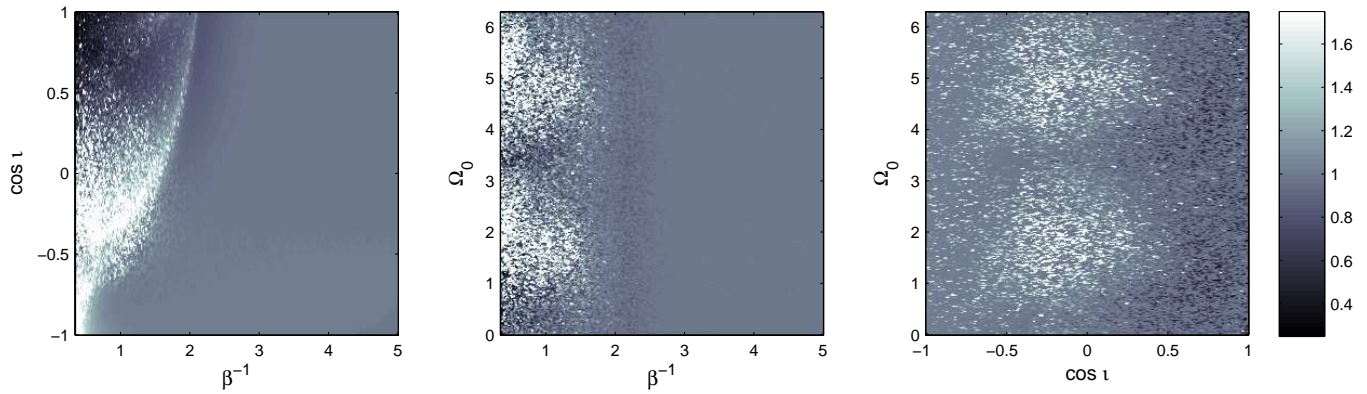


FIG. 13.— Resulting semi-major axis ( $a/a_0$ ) for surviving binaries plotted as intensity maps vs. pairs of input parameters. All values have been averaged over  $\theta_0$ .

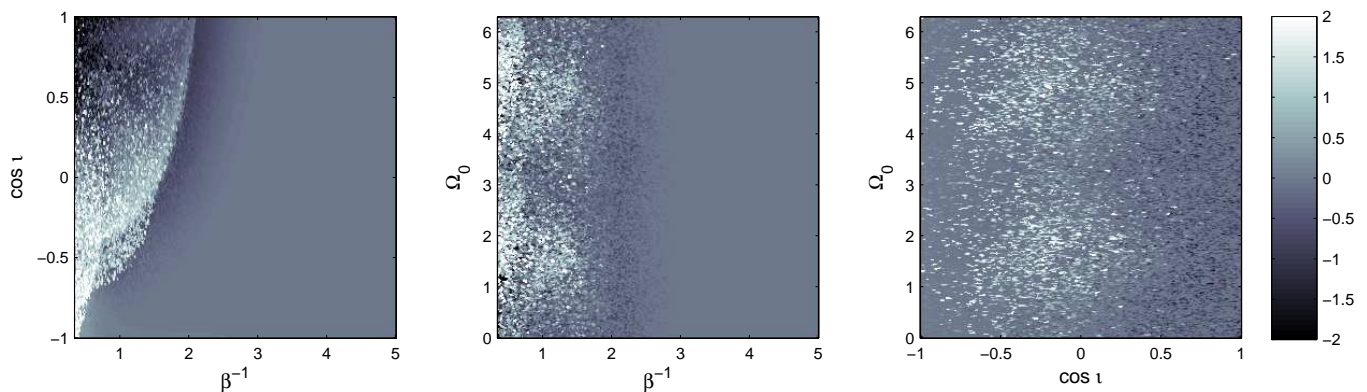


FIG. 14.— Gray scale maps of the Peters lifetime  $\log(\tau_{\text{gw}}/\tau_{\text{gw},0})$  for surviving binaries vs. pairs of input parameters. All values have been averaged over  $\theta_0$ .

subclass of surviving binaries for which  $\tau_{\text{gw}} < \tau_{\text{gw},0}$  those with a small enough BH orbital period such that they will not merge before completing one orbit are the “short period” BEMRIs, and understanding their full evolution requires a more careful (i.e. Post-Newtonian) approach to the integration in order to account for eccentricity and semi-major axis change due to GW loss during the long orbit. Both the unbound binaries and the long period BEMRIs which will merge before one SMBH orbit are factored into the calculation for the CBC rate enhancement, which is potentially important to ground based

GW detectors such as LIGO. We find that for the aLIGO volume, the enhancement factor for BH-BH mergers is  $\mathcal{E}_{CBC} \approx 0.25 \text{ yr}^{-1}$  or as much as 1% of the predicted rates, though this enhancement may be difficult to statistically detect in accumulated event catalogs.

PL supported by NSF grants 1205864, 1212433, 1333360. EA and SLL supported by NSF grant PHY-0970152, and from NASA award NNX13AM10G.

#### REFERENCES

- Abadie, J., Abbott, B. P., Abbott, R., Abernathy, M., Accadia, T., Acernese, F., Adams, C., Adhikari, R., Ajith, P., Allen, B., & et al. 2010, *Classical and Quantum Gravity*, 27, 173001
- Alexander, T. 2005, *Phys. Rep.*, 419, 65
- Amaro-Seoane, P., Gair, J. R., Freitag, M., Miller, M. C., Mandel, I., Cutler, C. J., & Babak, S. 2007, *Classical and Quantum Gravity*, 24, R113
- Antonini, F., Faber, J., Gualandris, A., & Merritt, D. 2010, *ApJ*, 713, 90
- Antonini, F., Murray, N., & Mikkola, S. 2014, *ApJ*, 781, 45
- Antonini, F., & Perets, H. B. 2012, *ApJ*, 757, 27
- Bromley, B. C., Kenyon, S. J., Geller, M. J., Barcikowski, E., Brown, W. R., & Kurtz, M. J. 2006, *ApJ*, 653, 1194
- Brown, W. R., Geller, M. J., Kenyon, S. J., & Kurtz, M. J. 2005, *ApJ*, 622, L33
- Edelmann, H., Napiwotzki, R., Heber, U., Christlieb, N., & Reimers, D. 2005, *ApJ*, 634, L181
- Ghez, A., Morris, M., Lu, J., Weinberg, N., Matthews, K., Alexander, T., Armitage, P., Becklin, E., Brown, W., Campbell, R., Do, T., Eckart, A., Genzel, R., Gould, A., Hansen, B., Ho, L., Lo, F., Loeb, A., Melia, F., Merritt, D., Milosavljevic, M., Perets, H., Rasio, F., Reid, M., Salim, S., Schödel, R., & Yelda, S. 2009, in *Astronomy*, Vol. 2010, astro2010: The Astronomy and Astrophysics Decadal Survey, 89
- Ghez, A. M., Salim, S., Hornstein, S. D., Tanner, A., Lu, J. R., Morris, M., Becklin, E. E., & Duchêne, G. 2005, *ApJ*, 620, 744
- Ghez, A. M., Salim, S., Weinberg, N. N., Lu, J. R., Do, T., Dunn, J. K., Matthews, K., Morris, M. R., Yelda, S., Becklin, E. E., Kremenek, T., Milosavljevic, M., & Naiman, J. 2008, *ApJ*, 689, 1044
- Gualandris, A., Portegies Zwart, S., & Sapior, M. S. 2005, *MNRAS*, 363, 223
- Hamilton, D. P., & Burns, J. A. 1991, *Icarus*, 92, 118
- . 1992, *Icarus*, 96, 43
- Heggie, D. C., & Rasio, F. A. 1996, *MNRAS*, 282, 1064

- Hills, J. G. 1988, *Nature*, 331, 687
- Hils, D., & Bender, P. L. 1995, *ApJ*, 445, L7
- Hopman, C., & Alexander, T. 2005, *ApJ*, 629, 362
- Ivanov, P. B. 2002, *MNRAS*, 336, 373
- Kalogera, V., Belczynski, K., Kim, C., O'Shaughnessy, R., & Willems, B. 2007, *Phys. Rep.*, 442, 75
- Kalogera, V., Narayan, R., Spiegel, D. N., & Taylor, J. H. 2001, *The Astrophysical Journal*, 556, 340
- Merritt, D., Alexander, T., Mikkola, S., & Will, C. M. 2011, *Phys. Rev. D*, 84, 044024
- Mikkola, S., & Aarseth, S. J. 1993, *Celestial Mechanics and Dynamical Astronomy*, 57, 439
- Mikkola, S., & Tanikawa, K. 1999, *MNRAS*, 310, 745
- Miller, M. C., Freitag, M., Hamilton, D. P., & Lauburg, V. M. 2005, *ApJ*, 631, L117
- Muno, M. P., Pfahl, E., Baganoff, F. K., Brandt, W. N., Ghez, A., Lu, J., & Morris, M. R. 2005, *ApJ*, 622, L113
- O'Leary, R. M., Kocsis, B., & Loeb, A. 2009, *MNRAS*, 395, 2127
- Peters, P. C. 1964, *Physical Review*, 136, 1224
- Raghavan, D., McAlister, H. A., Henry, T. J., Latham, D. W., Marcy, G. W., Mason, B. D., Gies, D. R., White, R. J., & ten Brummelaar, T. A. 2010, *ApJS*, 190, 1
- Scott, D. W. 1979, *Biometrika*, 66, pp. 605
- Sigurdsson, S., & Rees, M. J. 1997, *MNRAS*, 284, 318
- Yu, Q., & Tremaine, S. 2003, *ApJ*, 599, 1129